

Surface Symmetry Energy

Pawel Danieliewicz

National Superconducting Cyclotron Laboratory and
Department of Physics and Astronomy, Michigan State University,
East Lansing, Michigan 48824, USA

(May 22, 2019)

Abstract

The symmetry term in the standard semiempirical formula for binding energy has a volume character. However, as we demonstrate, the description of binding energies for light nuclei requires an inclusion of the surface symmetry energy in the binding-energy formula. The symmetry volume and surface energies combine in the formula like energies of two capacitors in parallel. A finite surface symmetry energy necessarily implies the existence of nuclear asymmetry skins, describable in terms of the ratio of symmetry energy volume parameter to an analogous surface parameter. Using available binding energy and skin data, we constrain the parameter values, finding 27 MeV . . . 32 MeV and 10.0 MeV . . . 12.5 MeV . We demonstrate in the Thomas-Fermi theory that the emergence of surface symmetry energy is related to the drop of symmetry energy per nucleon S with density and we constrain that drop, at half of the normal density ρ_0 , to 0.56 . $S(\rho_0/2) = S(\rho_0) - 0.81 (S(\rho_0))$. We examine modifications to the nuclear asymmetry vibrations produced by the emergence of surface asymmetry. We demonstrate that the giant dipole resonance changes its nature from a surface to a volume mode as the nuclear mass increases.

Keywords: binding energy formula, symmetry energy, surface symmetry energy, nuclear skin, giant resonance

PACS numbers: 21.10.Dr, 21.10.Gv, 21.60.Ev, 21.65.+f

Typeset using REVTEX

I. INTRODUCTION

Changes in the nuclear properties and in reaction dynamics under the changing nucleon content within a system attract attention in the context of the exotic nuclear beams [1]. Determination of the density dependence of symmetry energy, describing the rise in nuclear energy with increasing asymmetry between neutrons and protons, could permit extrapolations to the limit of neutron matter and determinations of neutron star properties [1,2]. The nuclei with a significant excess of neutrons over protons tend to be characterized by larger radii for the neutron than proton distributions, i.e. exhibit neutron skins. It has been noted, within nuclear mean-field calculations [3,6], that the skin size, in particular, could provide information on the density dependence of the symmetry energy.

Most elementary information on nuclear properties stems from the semiempirical energy formula describing the average changes in nuclear binding energy with the nucleon content [7,8]. The volume and surface terms in the standard formula pertain to symmetric systems. The volume coefficient provides the binding energy per nucleon in the symmetric nuclear matter; the surface coefficient, up to a factor, provides the surface tension. Notably, the symmetry term in the standard energy formula has a volume character only. However, elementary arguments indicate that the surface tension should depend on particle asymmetry. In this paper, we explore the consequences of such dependence. We demonstrate that, besides a modification of the energy formula to include the surface symmetry energy, the dependence necessarily implies an emergence of the asymmetric skin. The particle asymmetry shifts between the interior and surface to minimize the energy in the ground state. With the addition of a single additional coefficient in the energy formula, we are able to improve the description of nuclear binding energies and obtain a description of the skin systematics.

Our considerations are completely elementary. Similar considerations may be applied to any macroscopic binary system with an interface, such as between two phases [9]. Notably, the surface symmetry energy is present in the nuclear droplet model [10] where the relative displacement of the nuclear neutron and proton surfaces is a basic model parameter and, as such, a starting point. However, the multitude of other details in that model, however otherwise useful, can easily shroud the generality of results on asymmetry. Additional difficulty is brought upon by different definitions of the surface energy there [11,12], leaving a possible room for our basic exposition. The minimal number of parameters in our treatment has a chance of making the quantitative conclusions robust.

As one application of our results, we show how the emergence of the surface asymmetry excess modifies the giant resonances in nuclei. As the nuclear size changes, the nature of the surface boundary condition for asymmetry vibrations changes. For the case of the giant dipole resonance, the vibration changes from one that is closer to the Goldhaber-Teller type [13] to one closer to the Steinwedel-Jensen type [14].

We constrain the symmetry volume and surface energy coefficients by using data on nuclear masses [15] and on neutron skins [16–23]. Within the Thomas-Fermi theory, we demonstrate that the emergence of surface symmetry energy is associated with the fall of symmetry energy per nucleon with density. Combining our constraints and the results from nuclear mean-field models in the literature [6], we constrain the low-density drop in the symmetry energy.

The paper is organized as follows. In the next section, we discuss the symmetry energy

within the binding-energy formula and we analyze known masses in terms of a modified formula to constrain the symmetry energy parameters. In Sec. III, we derive an expression for the nuclear skin size in terms of the symmetry parameters and we analyze data on skins to obtain additional constraints. The asymmetry oscillations are discussed in Sec. IV. Connections to the microscopic theory are established in Sec. V. Our results are recapitulated in Sec. VI.

II. BINDING ENERGY FORMULA

A. Elementary Considerations

We start out with a reminder of elementary issues. The Weizsäcker nuclear energy formula [7,8]

$$E = a_V A + a_S A^{2/3} + a_a \frac{(N - Z)^2}{A} + a_C \frac{Z(Z - 1)}{A^{1/3}}; \quad (1)$$

separates out different contributions to the nuclear energy. The negative r.h.s. volume term represents the energy in the bulk limit of symmetric nuclear matter in the absence of Coulomb interactions. Proportionality to the mass number A for that largest in magnitude term, together with an approximately constant nucleon density $\rho_0 = 3 = (4 \pi r_0^3) / 0.160 \text{ fm}^{-3}$ in the nuclear interiors, underscore the short-range nature of nuclear interactions. The three subsequent terms in the Weizsäcker formula represent an increase in the energy compared to the bulk symmetric limit. Those terms are associated with the surface, with an asymmetry in the number of protons Z and neutrons N and with the Coulomb repulsion, respectively. Regarding the (a)symmetry term in the Weizsäcker formula, we observe that this term scales like A when the nucleon number is changed and that we do not have a surface (a)symmetry energy term, scaling like $A^{2/3}$. The $N - Z$ asymmetry reduces the binding because of the enhanced role of Pauli principle and because the like-nucleon interactions are less attractive than the neutron-proton interactions.

With the radius of the volume per nucleon r_0 , the size of the nuclear surface is $S = 4 \pi r_0^2 A^{2/3}$, and we can write the surface energy as

$$E_S = a_S A^{2/3} = \frac{a_S}{4 \pi r_0^2} S; \quad (2)$$

The tension is the derivative of energy with respect to surface area:

$$= \frac{\partial E}{\partial S} = \frac{a_S}{4 \pi r_0^2}; \quad (3)$$

The tension represents a work per unit area needed to create the surface. The work is required because the nucleons at the surface are less bound than in the interior. However, we know that the $N - Z$ asymmetry reduces the interior binding. Thus, with an increasing asymmetry, the work required per unit surface, the tension, should drop. Coulomb effects will also affect the surface, but will be dealt with later.

As a microscopic quantity, the tension should depend on a microscopic quantity associated with the particle asymmetry. The respective quantity common for different subsystems in contact is the chemical potential. With the nucleon chemical potentials given by

$$n = \frac{\partial E}{\partial N} \quad \text{and} \quad p = \frac{\partial E}{\partial Z}; \quad (4)$$

the potential conjugate to the asymmetry $N - Z$ is half of the nucleon potential difference, $a = (n - p)/2$, and the change in energy associated with the particle numbers is:

$$dE = n dN + p dZ = dA + a d(N - Z); \quad (5)$$

with the average chemical potential $= (n + p)/2$.

Given that the tension should drop no matter whether a neutron or proton excess develops, the tension needs to be, in lowest order, quadratic in the asymmetry potential a :

$$= 0 \quad \frac{2}{a} \quad (6)$$

where > 0 . As tension is a derivative of the surface energy, the dependence of γ on a implies the dependence of the surface energy on a , with serious consequences. To demonstrate these, let us construct the thermodynamic potential generated by the Legendre transformation from the asymmetry $N - Z$ to the potential a :

$$= a(N - Z) \quad E = a(N - Z) - E_V - E_S; \quad (7)$$

where we separated the energy into the volume E_V and surface E_S contributions. Partial derivative of γ with respect to a gives a net asymmetry in the nucleus $N - Z$. Let us consider a change in γ as we alter the asymmetry potential at constant A . Then, the volume energy change is $dE_V = a d(N_V - Z_V)$, where $d(N_V - Z_V)$ is the change in the particle asymmetry within nuclear volume, expected to be equal to $d(N - Z)$. From $N - Z = \gamma = \gamma_a$, we get:

$$a \frac{\partial(N - Z)}{\partial a} - \frac{\partial(N_V - Z_V)}{\partial a} - \frac{\partial E_S}{\partial a} = 0; \quad (8)$$

From the above, we see that if the surface energy is to depend on the chemical potential, then the nuclear interior cannot contain the whole particle asymmetry and some of it must, consequently, reside within the nuclear surface. To tackle the issue of how the surface can contain a particle number, we must consider how the surface quantities get to be defined.

For an interface between phases in equilibrium, Gibbs [9] suggested to take a small but macroscopic volume surrounding an element of the interface and, besides the actual system, consider an idealized reference system, cf. Fig. 1. In the idealized system, the densities of thermodynamic quantities, such as the particle density, change abruptly at the interface from a value characterizing one of the phases away from the interface to the value for the other phase. The surface share F_S for the surface element S is then the difference between the value of the quantity for an actual system F and the value for an idealized system F_{id} : $F_S = F - F_{id}$. In terms of densities, for the case of a nucleus in equilibrium with the vacuum, this further yields for a quantity F : $F_S = f_S = F - V f_V$, where f_V is the density of F characteristic for the interior and f represents the surface density. The problem is, however,

that the result for the surface depends on a precise position assumed for the interface, and a condition may be imposed further to specify the position. For a nucleus it is natural to assume that the surface contains no mass number and, for a spherical nucleus, this is equivalent to taking the equivalent sharp-sphere radius for the surface of $R = r_0 A^{1/3}$.

Only one condition related to the particle numbers, however, suffices to localize the surface. In a two-component system, the attempts to localize the surface using one of the components or the other would lead to two different positions. If the surface is localized using the net particle density, a finite surface asymmetry $N_S - Z_S$ results, even though the surface has a vanishing net nucleon number $A_S = N_S + Z_S = 0$. For a spherical nucleus, this corresponds to having two different equivalent sharp-sphere radii for neutrons R_n and protons R_p , bracketing the sharp-sphere radius for the matter R , cf. Fig. 2.

We will now relate the surface asymmetry excess to the asymmetry potential. With the surface quantities obtained from the Gibbs prescription, under the variation of asymmetry and of the volume surrounding the surface, we find

$$dE_S = dS + a d(N_S - Z_S) : \quad (9)$$

From changes in E_S , when taking an increasing fraction of the surface, we find that

$$E_S = S + a (N_S - Z_S) : \quad (10)$$

On taking a differential of the above and using the preceding relation we find

$$\frac{N_S - Z_S}{S} = \frac{d}{d_a} = 2 - a ; \quad (11)$$

where, in the last step, we employed Eq. (6).

With (11) and (6), we get from (10):

$$E_S = E_S^0 + \frac{1}{4} \frac{(N_S - Z_S)^2}{S} = E_S^0 + \frac{(N_S - Z_S)^2}{A^{2/3}} ; \quad (12)$$

where E_S^0 is the surface energy in absence of the surface asymmetry. We may note that, while the surface tension decreases with an increase in the asymmetry, Eq. (6), the net surface energy increases with the asymmetry. In the last step in (12), we introduced the constant with the dimension of energy, replacing , for the sake of an analogy with the representation for the volume energy suggested by (1):

$$E_V = E_V^0 + \frac{(N_V - Z_V)^2}{A} : \quad (13)$$

In the volume energy, we use in place of a_a of (1) to make a distinction between the symmetry constant in the bulk and the constant in use in the binding energy formula. As will be seen, a_a in use generally results from a combination of and .

Minimization of the net energy E under the constraint of net asymmetry,

$$E = E_V + E_S \quad \text{with} \quad N - Z = N_V - Z_V + N_S - Z_S ; \quad (14)$$

yields the condition of equal chemical asymmetry potentials for the interior and surface. Given (12), (13) and (14), the energy, in regard to asymmetry, takes the form such as

for connected springs, with the constants $=2A$ and $=2A^{2=3}$, respectively, or, even more appropriately, such as for capacitors with the capacitances of $A=2$ and $A^{2=3}=2$. Equality of the potentials demands that the asymmetries are in proportion to the capacitances:

$$\frac{N_S}{N_V} \frac{Z_S}{Z_V} = \frac{1}{A^{1=3}} \quad \text{and} \quad \frac{N_S}{N} \frac{Z_S}{Z} = \frac{\frac{A^{2=3}}{A + A^{2=3}}}{1 + -A^{1=3}} = \frac{1}{1 + -A^{1=3}}; \quad (15)$$

where in the right-hand result we use the net capacitance. The net energy is given in terms of the net capacitance and net asymmetry as

$$E = E_V + E_S = E^0 + \frac{(N - Z)^2}{A + A^{2=3}} = E^0 + \frac{(N - Z)^2}{1 + -A^{1=3}} \frac{A}{A}; \quad (16)$$

where E^0 stands for other, than the symmetry, terms in energy.

The symmetry energy of (16) should, generally, replace that in the energy formula (1), with $! 1 (! 0$, in (6)) obviously corresponding to the standard formula. In (15), we observe that the surface fraction of the asymmetry excess decreases as nuclear mass increases, because the surface capacitance grows only as $A^{2=3}$. It may be tempting to expand the symmetry energy (16) in the fraction. However, whether this can be done depends on the volume-to-surface coefficient ratio $=$. For large enough ratios and small A , we, in fact, principally might be able to ignore 1 in the denominator and get the symmetry energy such as characteristic for the surface storage of asymmetry. This would express the fact that, just as the volume capacitance grows faster than surface capacitance, it also drops faster. Later in this and in the following section we shall see what $=$ values are favored by data.

B. Coulomb Effects

So far, we have not considered the effect of Coulomb interactions on the surface asymmetry and the Coulomb and symmetry energies interplay in the net energy. The Coulomb energy may be represented as

$$\begin{aligned} E_C = E_V^C + E_{VS}^C + E_S^C &= \frac{e^2}{4\pi_0 R} \frac{1}{5} \left(\frac{3}{5} Z_V^2 + Z_V Z_S + \frac{1}{2} Z_S^2 \right) \\ &= \frac{a_C}{A^{1=3}} \left(\frac{5}{3} Z_V^2 + \frac{5}{6} Z_V Z_S + \frac{5}{6} Z_S^2 \right) \end{aligned} \quad (17)$$

where the three terms correspond to the volume, volume-surface and surface interactions, respectively, and $Z_V = Z - Z_S$.

The combination of symmetry energies (12) and (13) and Coulomb energy (17) is quadratic in the surface excess and is easily found to minimize at:

$$N_S \frac{Z_S}{Z} = \frac{N - Z - \frac{a_C}{12} Z A^{2=3}}{1 + -A^{1=3} + \frac{a_C}{48} A^{2=3}} \frac{N - Z - \frac{a_C}{12} Z A^{2=3}}{1 + -A^{1=3}}; \quad (18)$$

The last approximation expresses the fact the Coulomb interactions represent a very soft spring in the energy combination, compared to the volume asymmetry spring. Compared

to (15), we see that, as might be expected, the Coulomb interactions try to tilt the surface asymmetry towards proton excess. Quantitatively, however, the Coulomb correction to the asymmetry excess is quite negligible for light and medium nuclei and acquires only a limited significance for heavy nuclei.

As to the energies, even when the Coulomb correction to the surface asymmetry has a significance, the corresponding changes in the asymmetry energy are quite ignorable. This is because around the minimum, specified by (15), the changes in the asymmetry energy are quadratic in the asymmetry correction. On the other hand, the correction to the Coulomb energy, from the development of the surface asymmetry,

$$E_C \sim \frac{\partial E_C}{\partial Z_S} \Big|_0 Z_S \sim \frac{a_C Z^2}{A^{1/3}} \frac{N - Z}{6Z} \frac{1}{1 + -A^{1/3}}; \quad (19)$$

may have a moderate significance and, in heavy nuclei, can reach a comparable magnitude to the correction to the Coulomb energy from surface diuseness.

C. Comparison to Binding-Energy Data

We now confront the above basic results with the data [15] on nuclear binding energies, $B = E - E_0$, that we fit with the formula of the form :

$$E = a_V A + a_S A^{2/3} + \frac{(N - Z)^2}{A} + a_C \frac{Z(Z - 1)}{A^{1/3}(1 + \dots)}; \quad (20)$$

Compared to (1), we changed the symmetry term to (16) and we added the standard pairing term $= -g_A A^{1/2} \cdot 0$. We either carry out fits with $= 0$ in the Coulomb term, i.e. the energy formula modified from the standard one only by the inclusion of surface symmetry energy, or with

$$= \frac{5}{6} \frac{d^2}{r_0^2 A^{2/3}} \frac{1}{1 + -A^{1/3}} \frac{N - Z}{6Z}; \quad (21)$$

including the effects of surface diuseness and of the asymmetry skin (19) on the Coulomb energy. In the first r.h.s. term above, $d = 0.55$ fm is the diuseness parameter in the Fermi function parametrization of nuclear charge distributions [24],

$$(r) = \frac{0}{1 + \exp[(r - c)/d]}; \quad (22)$$

and this term stems from an expansion of the Coulomb energy for (22) in terms of d .

Qualitatively, results of the two fits indicated above are similar but they differ in quantitative details. Obviously, the inclusion of the volume and surface competition in the symmetry energy, changes the dependence of the net energy on asymmetry as a function of mass. However, the Coulomb energy is also a source of the dependence on asymmetry and deciding on details in one energy contribution depends on the details in the other. We believe that more reliable results are obtained with the fits (21) in (20) as we only incorporate information available from electron scattering or following from the intrinsic consistency of

considerations. The number of independent parameters in the t with (21) is the same as in the other t , precluding, in practice, running away of the t in the parameter space.

In the t s, we optimize the sum of absolute deviations of the theoretical from experimental energies, rather than the sum of deviations squared, as the intention is to provide an average description of nuclear features. Results, however, weakly depend on that choice. We either let all parameters vary in an unconstrained manner or we constrain $=$ or both of the symmetry parameters.

The average per nucleus deviation of energy from experimental values exhibits a narrow valley in the space of $=$ vs $=$, as illustrated in Fig. 3 for the t with (21). The valley is described by $(21.5 + 3.1 =) \text{ MeV}$. An analogous valley is found for the t with $= 0$, but the valley is shifted by about 10% to higher values in $=$. The strong correlation may be understood in terms of the need to properly describe energies for the heaviest nuclei with largest asymmetries requiring $= (1 + A^{-1/3}) = a$, for $A \approx 200$.

Along the valley, the average deviation minimizes at $= 1.7$. However, the minimum in that direction is rather flat. To understand the nature of the minimum, we carry out the following procedure. We carry out an optimization of all parameters in the energy formula at a fixed $=$. Then keeping all parameters fixed, including $=$ but excluding $=$, we invert the energy formula to deduce $=$ from the mass of an individual nucleus. With this, we test locally the global t . If the formula provides a proper description, then on the average we should get the same $=$ from an individual mass as from the global t . Notably, for the inversion to be significant, the asymmetry should be large and we demand that $\frac{N}{Z} \frac{A}{Z} > 0.2$. Sample results are displayed in Fig. 4, as a function of A .

First to consider are the results obtained at $= = 0$, i.e. ignoring the surface symmetry energy, as common in the mass formulas. Represented by the diamonds in Fig. 4, the results for $=$ (i.e. a_a in this case) group coarsely into a line. At large A , the line from symbols oscillates, exhibiting the shell structure, around the value of $=$ from the global t , represented by a straight line. However, at $A \approx 50$ the values from inversion systematically drop below a_a from the global t . Such a drop for a_a at low A is expected from a competition between the volume and surface symmetry energies (20). If we raise the parameter ratio, such as to the value of $= = 2$, we can get the locally restored values of $=$ to oscillate around the global t value down to very low A . Regarding the restored values of $=$, we may note in Fig. 4 that they locally exhibit less scatter for t s with (21) than with $= 0$, suggesting that the first t grasps the physics better. Finally, if we assume a too high value of the parameter ratio, such as $= = 6$, we get the restored $=$ to raise up at low A in an opposite tendency to that for $= = 0$.

While, at the lower A , the use of an intermediate value of $=$ improves the performance of the energy formula, at the highest A the separate sensitivity to the ratio is quite reduced. With most of the measured nuclei of high anisotropies at the high A , the reduction in the deviation between the formula and the experimental energies, when averaged over all A , is just 0.40 MeV per nucleus for the absolute minimum in Fig. 3 compared to the optimal case of $= = 0$. Considering in particular Fig. 4, we need to decide how accurate our phenomenological theory should be in describing the nuclei. While the superiority of the $= = 2$ case over the other cases in Fig. 4 is quite apparent, cases that might be less than a third of the way in-between $= = 2$ and the two other would not be clearly superior, given the scatter of the points and the lack of description of shell effects in the theory. With this,

we consider the locus of points in the (Δ, Δ) plane corresponding the deviation reduced by a factor of $1/3$ compared to the optimal $\Delta = 0$ point (i.e. 0.13 MeV in Fig. 3), as the approximate boundary of the parameter range favored by the energy formula. Have we had a theory that could e.g. predict the shell effects, we might have been able to impose a more stringent limit on the parameters. For reference, we further show in Fig. 3 the boundary for the 0.40 MeV deviation passing through the optimal $\Delta = 0$ point and in the vicinity of the optimal $\Delta = 6$ point.

Before we turn to the discussion of asymmetry skins, of which thickness is a primary variable in the droplet model [10], let us make contact with the notation there. Our two asymmetry parameters in terms of those in the droplet model are [11]:

$$\Delta = J \quad \text{and} \quad \Delta = \frac{4}{9}Q = \frac{\frac{4}{9}H}{1 - \frac{2}{3}P = J} : \quad (23)$$

III. ASYMMETRY SKINS

Interest in asymmetry skins has surged in the context of the general interest in asymmetry effects, stemming from the availability of radioactive beams. Expectations were raised that an analysis of the asymmetry skins could permit to extrapolate the nuclear matter properties to the neutron matter [36]. Different features of effective interactions have been tested with regard to their bearing on the thickness of the skins. In several works [25], a direct connection between the neutron skin in the spherical ^{208}Pb nucleus and the neutron star structure was made.

Unfortunately, experimental extraction of the neutron distributions has been difficult. Different methods have been employed, such as analyses of nucleon scattering [16,17,22,23] (including the analysis of polarized proton scattering and of neutron and proton scattering) or analyses combining information from strongly interacting ($p, \pi, \gamma, ^{12}\text{C}$) and electromagnetic probes (e scattering, isotopic transition shifts) [18-21]. Recently, it has been proposed [26] to utilize parity violations in electron scattering to determine neutron rms radii, contributing to the surge of interest in the asymmetry skins.

To assess the thickness of the asymmetry skin for a given surface excess (18), let us consider the sharp sphere radii for the neutrons R_n and protons R_p . These radii correspond to volumes with interior densities such as for the bulk matter, i.e.

$$N = \frac{N_V}{A} = \frac{4}{3} R_n^3 = N_V \left(\frac{R_n}{R} \right)^3, \quad N_V = 1 + \frac{3(R_n - R)}{R} : \quad (24)$$

In the last step, we use the fact that the intrinsic consistency of our considerations requires that we can tell the surface from the interior and thus must have $R_n > R_p$ and R or, equivalently, $N_s > Z_s$. We next get from (24)

$$\frac{R_n - R}{R} = \frac{N_s}{3N} : \quad (25)$$

With an analogous result for R_p , we find for the difference of the sharp-sphere radii:

$$\frac{R_n - R_p}{R} = \frac{A (N_s - Z_s)}{6N Z} = \frac{A}{6N Z} \frac{N - Z - \frac{a_c}{12} Z A^{2/3}}{1 + - A^{1/3}} : \quad (26)$$

We see that the difference between the neutron and proton radii is primarily linear in the asymmetry and measures the symmetry coefficient ratio $\alpha = \frac{N_s - Z_s}{N + Z}$. For a surface with no capacitance for the asymmetry, characterized by $\alpha = 0$, the asymmetry skin should vanish.

Regarding (26), the results of measurements and of microscopic calculations for the skins are, however, not usually expressed in terms of a difference of the sharp sphere but rather of the rms radii for neutrons and protons. The difference between the rms compared to the sharp sphere radii, aside from the standard reduction factor (dropping out from the ratio of radii) and from a correction for the usefulness, brings in a Coulomb correction additional to that already in (26). That correction stems from a polarization of the nuclear interior by the Coulomb forces. The polarization is schematically indicated in Fig. 2. In order to assess the polarization effect, we represent the interior symmetry and Coulomb energies in a local form, within the net nuclear energy. We expand those energies, respectively, to the second and first order in the deviation from uniformity:

$$E = E^0 + \int_0^Z dr (a_a)^2 \frac{1}{2} dr (r) \quad a_a : \quad (27)$$

Here, E is the Coulomb potential, a_a is the neutron-proton density difference, $a_a = n_p - p_n$, and we exploit the relation for the density changes $p_p = -a_a/2$ following from the requirement $n_n + p_p = 0$. The energy E^0 is the remaining portion of the energy minimized with respect to the global partition of the asymmetry between the interior and surface. The minimization of (27) with respect to a_a , under the constraint of $dr a_a = 0$, yields

$$\overline{a_a(r)} = \frac{1}{4} \overline{(r)} - = \overline{0} \frac{a_c}{8} \frac{Z}{A^{1/3}} \quad 1 \quad \frac{5}{3} \frac{r^2}{R^2} ; \quad (28)$$

where the overline indicates an average over the interior volume and where we use the sharp-sphere potential. On calculating the contribution from (28) to the difference of the rms neutron and proton radii, we find

$$\frac{\overline{hr^2 i_n^{1/2}} - \overline{hr^2 i_p^{1/2}}}{\overline{hr^2 i^{1/2}}} = \frac{a_c}{168} \frac{A^{5/3}}{N} : \quad (29)$$

Notably, the contribution from the polarization (28) to the net energy is practically ignorable.

On combining (26) with (29) and on incorporating a correction for the surface usefulness into (22), we get for the difference of the neutron and proton rms radii:

$$\frac{\overline{hr^2 i_n^{1/2}} - \overline{hr^2 i_p^{1/2}}}{\overline{hr^2 i^{1/2}}} = \frac{A}{6N Z} \frac{N - Z}{1 + - A^{1/3}} \quad \frac{a_c}{168} \frac{A^{5/3}}{N} \frac{\frac{10}{3} + - A^{1/3}}{1 + - A^{1/3}} + \frac{2}{hr^2 i} \frac{d(d_n - d_p)}{hr^2 i} : \quad (30)$$

Calculations [3] appear to indicate that, for lighter nuclei, the difference in the neutron and proton usefulness $d_n - d_p$ is of the second order in the difference of sharp-sphere radii (26). For heavy nuclei, there may be a Coulomb contribution to the difference in the usefulness.

Overall, in any case, the correction for di useness, to the skin thickness, is of a lower order in Λ than the leading term.

In Fig. 5, we compare the results of skin measurements in Na isotopes [21] to the results from (26) for different assumed values of γ , with the difference in di useness set to zero and with γ made to follow the binding-energy correlation valley in Fig. 3. The data rather clearly rule out $\gamma < 1$, but it is difficult, so far, to determine the energy parameter ratio with a much better precision. Further comparisons to data are shown in Figs. 6 and 7, for Sn and Pb isotopes, respectively. Overall, the displayed data appear to favor the ratios in the vicinity of $\gamma = 3$. As the charge number increases, one can see in Figs. 5–7, at $\gamma = 0$, the increasing importance of Coulomb corrections to the skin size. For a realistic $\gamma = 3$, we find that the Coulomb forces contribute about 0.07 fm of reduction to the skin of ^{208}Pb . This can be compared to the 0.1 fm change in the skin size found by Furnstahl [6] for ^{208}Pb when switching off the Coulomb interactions in mean-field models. The interior polarization and pushing out of the proton surface by the Coulomb interactions contribute about evenly to the skin reduction in our estimates.

It needs to be mentioned that, when different methods are employed in skin extraction from measurements, such as in the case of Ca isotopes [16{19,23], the outcomes can easily differ by more than the claimed errors, underscoring the difficulty in extractions. Results from a global fit of (30) to the available skin sizes obtained from data [16{23] are next shown in terms of contour lines in Fig. 3. As has been already discussed, the dependence of skin sizes on asymmetry primarily constrains the values of the ratio γ . We provide the contours for two combinations of a standard statistical deviation and an assumed average theoretical error of (30), i.e. $\sigma^2 = \sigma_{\text{min}}^2 + 1 + \sigma_k^2$ ($k = 1$)² where k is data index, and $\sigma = 0.02$ or 0.04 fm.

As evident in Fig. 3, the global fit to skin sizes constrains the ratio γ to a relatively narrow range of 2:1. $\gamma = 3.2$. As we will later see, at a microscopic level the γ ratio is related to the density dependence of the symmetry energy and, thus, these constraints constrain further the density dependence of the energy. Including the constraints from the binding energy systematics, we see in Fig. 3 that the value of the symmetry energy at normal density can be constrained to within the range 27 MeV . . . 32 MeV . However, in detail, the acceptable values of γ are correlated to $\gamma = 3$.

In the next section, we employ our elementary results in a description of the asymmetry oscillations in nuclei.

IV. APPLICATION TO ASYMMETRY OSCILLATIONS

A. Goldhaber-Teller and Steinwedel-Jensen Models of the Giant Dipole Resonance

So far, we discussed the elementary static properties of ground-state nuclei. Nuclear excitations may involve displacements of protons relative to neutrons, compared to the ground state, with prominent giant resonance structures in cross sections allowing for an interpretation in terms of a collective motion involving a number of nucleons. The lowest in energy (or frequency) is the giant dipole resonance (GDR) prominent in the low-energy photoabsorption [27] and inelastic electron scattering [28] cross sections.

Two early models have been advanced for GDR, under the names of Goldhaber and Teller (GT) [13] and Steinwedel and Jensen (SJ) [13,14]. In the GT model, the neutron and proton distributions are assumed to oscillate against each other as rigid entities, see Fig. 8. Since the energy associated with the displacement is proportional to the nuclear surface area, i.e. $\propto A^{2/3}$, while the moving mass is proportional to A_p , the resonance excitation energy in this model is proportional to $A^{1/6}$: $E_{GDR} \propto \frac{1}{A^{2/3}} = A^{-1/6}$. In the SJ model, a standing wave of neutron vs proton displacement develops within the nuclear volume, satisfying the surface condition of vanishing asymmetry u_x , analogous to the close pipe condition in the standard example of oscillations of a continuous medium. As the wavelength is then in a definite constant ratio to the nuclear radius, the resonance energy in the model is proportional to $A^{1/3}$: $E_{GDR} \propto c_a = A^{1/3}$, where c_a is the speed of propagation for asymmetry perturbations in normal symmetric matter.

In detail, within the SJ model [14,29], it is assumed that there is no net momentum of matter, i.e. the net matter velocity v vanishes and the net nucleon density stays intact, consistent with the continuity equation: $\frac{\partial}{\partial t} (n_p - p_n) = 0$. The relative density $a = n_p - p_n$ changes, but the state of matter is locally the same as in a ground-state nucleus, just at the new asymmetry. The vanishing net velocity implies a relation between the velocities for individual particles, v_n and v_p , and densities, following from the consideration of fluxes

$$0 = v = n v_n + p v_p : \quad (31)$$

This then implies that the flux in the asymmetry continuity equation may be expressed in terms of the relative velocity $v_{np} = v_n - v_p$,

$$\frac{\partial}{\partial t} a = r (n v_n - p v_p) = r \frac{2(n_p - p_n)}{m} v_{np} , \quad \frac{2N Z_0}{A^2} r v_{np} : \quad (32)$$

where the approximate equality is valid in the lowest order in the disturbance. An Euler type equation for the relative velocity can be next used to close the equation above,

$$\frac{\partial}{\partial t} v_{np} = \frac{2}{m} r a = \frac{2}{m} \frac{\partial}{\partial a} r a = \frac{2 c_a^2}{m} r a ; \quad (33)$$

where m is the effective mass and

$$c_a^2 = \frac{m}{m_0} \frac{\partial}{\partial a} a : \quad (34)$$

On differentiating Eq. (32) with respect to time and on substituting (33), we get the wave equation for the asymmetry density

$$\frac{\partial^2}{\partial t^2} a = \frac{4N Z_0}{A^2} c_a^2 r^2 a : \quad (35)$$

Under spherical symmetry, the normal vibrations are looked for, in the standard way, in terms of the deviation from ground-state density expressed as the product of a spherical Bessel function j_ν and a spherical harmonic Y_m ,

$$a = C_V \sin(\nu t) j_\nu(qr) Y_m(\theta) ; \quad (36)$$

where the wavenumber q and the frequency ω are related by

$$\omega = \frac{2 \frac{p}{N Z}}{A} c_a q; \quad (37)$$

The radial velocity component, from (33), is

$$v_{np}^r = \frac{2C}{0} \frac{A}{2 \frac{p}{N Z}} c_a \cos(\omega t) j_n^0(qr) Y_m(\theta); \quad (38)$$

The condition that the normal component of u_x vanishes at the surface [30], $v_{np}^r(R; \theta) = 0$, yields the wavenumber values

$$q_n = \frac{j_n^0}{R}; \quad (39)$$

where n orders the values and j_n^0 represents the n 's zero of the spherical Bessel function derivative, $j_n^0(j_n^0) = 0$. For the resonance energy, we get, given (37),

$$E_n = \omega_n = \frac{2 \frac{p}{N Z}}{A} \sim c_a q_n = \frac{2(NZ)^{1/2}}{A^{4/3}} \frac{\sim c_a j_n^0}{r_0}; \quad (40)$$

where, with (34) and (13),

$$c_a = \frac{r}{\frac{2}{m}} : \quad (41)$$

The GDR is characterized by $\gamma = 1$ and $n = 1$. With $j_{11}^0 = 2.08$, the GDR energy in the SJ model is then, finally,

$$E_{GDR} = \frac{2(NZ)^{1/2}}{A^{4/3}} \frac{2}{m} \frac{1/2}{r_0} \frac{2.08}{r_0} \sim \frac{2}{m} \frac{1/2}{r_0 A^{1/3}} \frac{2.08}{r_0} : \quad (42)$$

Within the GT model of the GDR, the changes in the asymmetry occur only within the nuclear surface and in the SJ model only within the interior. Experimental dependence of GDR energy on mass number, displayed in Fig. 9, is intermediate [27] between that characteristic for the GT and SJ models, suggesting that both the volume and surface participate in the oscillations. To explain the mass dependence of the GDR energy, in Ref. [31], the oscillation in the SJ model was treated as an elementary mode of nuclear oscillation and was coupled to a second GT mode of oscillation within the same nucleus. As the resonance frequencies for the two models, GT and SJ, shifted with a changing nuclear mass, the lower-frequency normal mode for the combination of oscillators changed from a mode with a predominantly GT to SJ content. However, this casts a nuclear system into one with only two degrees of freedom. The physical situation is rather that of a continuous system for which, though, the surface can generally accept the asymmetry u_x , making the SJ boundary condition excessively restrictive.

B . D escription of A sym m etry O scillations

We now explore the modification and consequences of the surface boundary condition for the asymmetry oscillations. Given that the surface can store an asymmetry excess, we replace the SJ condition of a vanishing ux with the condition for the change in surface asymmetry density n_a ,

$$\frac{\partial}{\partial t} n_a = n_v^r - p_v^r = \frac{2N Z_0}{A^2} v_{np}^r; \quad (43)$$

cf. (32). As the chemical potential for the surface needs to be the same as within the adjacent interior, this can be further rewritten as a condition involving the interior chemical potential, or involving the volume density next to the surface,

$$\frac{\partial}{\partial t} n_a = \frac{\partial n_a}{\partial t} \frac{\partial \phi_a}{\partial t} = \frac{\partial n_a}{\partial t} \frac{\partial \phi_a}{\partial a} \frac{\partial a}{\partial t} = \frac{2N Z_0}{A^2} v_{np}^r; \quad (44)$$

When the surface does not accept the excess, i.e. $\partial n_a / \partial t = 0$, we get the regular SJ condition of a vanishing ux.

Looking for normal modes with (36) and

$$n_a = C_s \sin(\omega t) Y_m(\theta); \quad (45)$$

we find from the equality of chemical potentials at the surface that

$$C_s = \frac{3}{A^{1/3}} C_v R j_0(qR); \quad (46)$$

Moreover, with (38), and (37), we can obtain from either (43) or (44) the condition for the wavevector

$$qR j_0(qR) = \frac{3}{A^{1/3}} j_0^0(qR); \quad (47)$$

As the ratio $= A^{1/3}$ grows from small to large values, the relative magnitude of the surface amplitude C_s in (46) grows. Moreover, it is apparent that the solutions to the wavenumber equation (47) generally shift then from $j_0^0 = R$ to $j_n = R$, where j_n represents the n 'th zero of the spherical Bessel function, $j_0(j_n) = 0$. In terms of the standard example of oscillations for a continuous medium, the boundary condition shifts from one representing a closed pipe to one representing an open pipe. At $A^{1/3} = 1/0$, however, the $n = 1, > 0$ solution to the wavenumber equation with $q \neq 0$, generally requires a careful expansion.

Let us now consider the $= 1$ GDR case. For $= A^{1/3} \neq 0$, the surface amplitude tends to zero and we get the SJ limit with the GDR energy given by (42). For $A^{1/3} = 1/0$, we need to consider the Bessel function in (47) at small values of its argument where $j_1(x)$ ($x=3$) ($1 - x^2=10$). We then find for the wavenumber

$$q_{11} = \frac{3}{r_0 A^{1/6}}; \quad (48)$$

and for the resonance energy

$$E_{GDR} = \sim!_{11} = \frac{2^P \overline{N Z}}{A} \sim c_a q_{11} = \frac{2(NZ)^{1=2}}{A^{7=6}} \frac{6}{m} \stackrel{1=2}{\sim} \frac{6}{m} \stackrel{1=2}{\sim} \frac{6}{r_0 A^{1=6}} : \quad (49)$$

In this limit, the resonance energy becomes dependent only on the surface symmetry parameter and not on the volume parameter. Moreover, the volume amplitude gets suppressed relative to the surface amplitude in (46). This is clearly the GT limit of vibration.

Figure 9 shows next fits to the data [27] on mass dependence of the GDR energy, with c_a treated as a fit parameter and with q_{11} obtained from (47) for different values of α . We see that a realistic ratio of $\alpha = 3$ yields a much better description of the data than the SJ ratio of $\alpha = 0$. However, a still larger ratio than 3 would provide an even better description. It is possible that other factors than the finite capacitance of the surface for asymmetry play here a role, such as local deviations of the system from a ground state [32].

One may ask for what values of A and realistic α the vibrations turn from more GT to more SJ like. As a criterion one may use the fraction of potential energy of the vibration attributable to the surface. With this criterion, one finds that the transition takes place at $A_{tr}^{1=3} = 3=2$, and, thus, for the range of 2:1. $\alpha = 3/2$, at 30. $A_{tr} = 110$. The relatively high transition masses are due to the requirement that the vibration must have a node at the center of the nucleus.

C. Transition Densities

The profile of the standing wave in oscillation represents, at the quantal level, the transition density for the resonance. This density is probed in inelastic electron scattering [28]. To our knowledge, no inversion of data for the GDR transition density has been made, but the data were tested against the GT and SJ type densities with a conclusion that the GDR (and also ' > 1 ') densities are in-between the two limits [28]. Even in theoretical works, the transition densities have not been much quoted.

We write the transition density as

$$_1(r) = _1(r) Y_m ; \quad (50)$$

where $_1(r)$ includes both the volume and surface contributions. Interpreting the volume results in terms of long-wavelength modulations of the particle densities and the surface results in terms of the modulations of radii, we have for the density [28]

$$_1(r) = \frac{1}{0} C_V j_1(qr) - C_S \frac{d}{dr} \quad (51)$$

where $\rho(r)$ is the ground-state density distribution. With (46), we can further rewrite this as

$$_1(r) = \frac{C_V}{0} j_1(qr) - (r) - \frac{3}{A^{1=3}} r \frac{d}{dr} ; \quad (52)$$

Establishing a contact with microscopic theory, we compare in Fig. 10 the GDR transition density for ^{40}Ca from (52) with (22) to the transition density from the microscopic

calculations of Ref. [33] which include effects of 2p-2h excitations and of ground state correlations. The normalization in (52) is obtained from the Thomas-Reiche-Kuhn sum rule; for illustrative purposes, we take $m = m$ as in [33]. The calculations [33] employ a phenomenological Landau-Migdal type interaction in use in describing different giant resonances and we note that a best contact with our results is made for $\alpha = 3$.

V. RELATION TO MICROSCOPIC THEORY

Several works tried to identify links between the asymmetry skins and bulk properties of nuclear matter associated with the asymmetry, within microscopic theory [36]. Having explored a link between the skins and the surface and volume symmetry parameters, we will now try to establish a connection between the parameters and the density dependence of the symmetry energy.

A. Symmetry Parameters in Thomas-Fermi Theory

We shall consider a nuclear energy functional expanded to the second order in asymmetry:

$$E = E_0 + \int dr S(r) - \frac{a}{E_0 + E_a} \quad (53)$$

Here we assume that the expansion term in asymmetry is local, but this will not be essential for much of the discussion that follows. The function S is the density-dependent symmetry energy per nucleon and $S(0) = 0$. The energy E_0 is generally nonlocal but independent of asymmetry as the zeroth order term in the expansion; since the Coulomb effects have been explicitly considered in Secs. II and III, we will disregard them for the discussion that follows. Regarding the role of asymmetry in any nonlocality, there had been indications [36] that it has a negligible impact on the properties of nuclei; the apparent success in systematizing the asymmetry skins in terms of the nuclear matter properties [36] lends, in itself, a support to the weak impact.

A simple example of the functional (53) is such as employed in the initializations of transport calculations for central reactions [34]:

$$E_0 = \int dr \left[\frac{3}{5} F + \frac{A}{0}^2 + \frac{B}{(0+1)}^2 + \frac{D}{2} \int dr (r^2) \right] \quad (54)$$

$$S = \frac{1}{3} F + \frac{C}{0} + \frac{F}{2}^2 ; \quad (55)$$

with the Fermi energy $F = (3^2 - 2^2)^{2/3} \approx 2^{2/3} = 2m$. The constants A , B and C are fixed by the requirement that the functional yields the energy minimum of $E = A = a_F = 16$ MeV at 0 in symmetric nuclear matter, that is characterized by some specific incompressibility constant K . E.g. for $K = 260$ MeV, we get $A = 180.9$ MeV, $B = 128.1$ MeV and $C = 1.446$. The constant D provides a size scale for the surface dimension and an adequate surface profile is obtained [34] for $D = 20.4$ MeV fm². As to the constants in S , we have the

relation $= F = 3 + C + F$ and, otherwise, different combinations of the constants C and D yield different values of α as will be discussed.

The minimization of the energy (53) under the conditions of fixed particle numbers

$$A = \int dr \quad \text{and} \quad N = \int dr \quad Z = \int dr \quad (56)$$

produces the Thomas-Fermi equations:

$$= \frac{E_0}{a} + \frac{2}{a} \frac{d}{dr} \frac{S}{Z} ; \quad (57)$$

$$_a = 2 \frac{S(0)}{a} : \quad (58)$$

At first, those equations will just serve as a background illustration for the claims made in the discussion.

On the basis of (53), we would like to find out changes in the nuclear ground-state energy, as the particle asymmetry changes. First, we consider a symmetric system and find (r) that minimizes the energy $E = E_0$. With the energy E being quadratic in asymmetry, the net density minimizing the energy functional at a finite asymmetry will differ from the density for the symmetric system only to within a second order in asymmetry. With this, to within the second order in asymmetry, a ground-state E_a in (53) may be calculated with (r) obtained for symmetric matter. Moreover, since the symmetric system (r) minimizes E_0 , any changes to it, of the second order in asymmetry, will produce only quartic terms of change in E_0 . In conclusion, if we are interested in the change in the ground-state energy to the second order in asymmetry, we just need to consider the E_a term in (53) and we can use there the density (r) from the energy E_0 minimized for a symmetric system. In terms of the Thomas-Fermi equations, this means that we can uncouple (57) by putting $\alpha = 0$ there.

From the second of the Thomas-Fermi equations, we have in the ground-state system

$$_a = \frac{a}{2} \frac{Z}{S} \quad (59)$$

and from (53)

$$E_a = \frac{a}{4} \int dr \frac{Z}{S} : \quad (60)$$

Within the analogy with a capacitor, the integral $\int dr (= 2S)$ represents the system capacitance, independent of the deposited charge. The volume capacitance is $A = 2$ and the remainder is the surface capacitance:

$$\frac{A^{2=3}}{2} \frac{S}{2 r_0^2} = \frac{1}{2} \int dr \frac{1}{S} \frac{1}{r} : \quad (61)$$

As we will not be pursuing here curvature effects, we just turn to the surface capacitance for a semi-infinite matter. With x a coordinate along the direction perpendicular to the surface

and on factoring out the density dependence from the symmetry energy with $S = s(=0)$, we find from (61)

$$- = \frac{3}{r_0} \int_0^Z dx \frac{1}{s} \quad 1 : \quad (62)$$

Thus, for (53), given that the density profile for the surface is constrained, the ratio of the symmetry parameters $=$ is a measure for the density dependence of the symmetry energy S . We note that a density-independent symmetry energy, characterized by $s = 1$, yields $= 0$. The falling density at the surface produces in this case no extra capacitance per nucleon compared to the interior. The faster the drop of s with density, the larger the extra capacitance, exhibited in a larger $=$ ratio.

We next test the validity of the considerations from Secs. II and III within a Thomas-Fermi model based on Eqs. (54) and (55), with a minor alteration, however, that the different neutron and proton Fermi energies are treated explicitly for asymmetric nuclei. On one hand, we solve the differential equation [34] from (57) for the semi-infinite symmetric matter and we vary C and F to get various combinations of $=$ from (62), requiring that they follow the binding-energy correlation from Fig. 3. Given the C and F values, we make a prediction for the size of the asymmetric skin of a specific nucleus, following Eq. (30) with $d_n = d_p = 0$. On the other hand, we solve the Thomas-Fermi equations directly for a nucleus, with Coulomb forces included, and calculate the difference of rms radii. A comparison of the results for N isotopes is shown in Fig. 11. The results are both compared when changing the isotope mass, while keeping the symmetry parameters fixed, and for one isotope when changing the symmetry parameters. As is seen, the agreement of the estimate (30) with the actual skin size is rather remarkable. For heavy nuclei, however, a small systematic difference develops between the actual and estimated skin sizes, that largely vanishes when the Coulomb forces are switched off. The size of the discrepancy, ~ 0.03 fm for Pb, for which we have no understanding, is compatible with the possible difference between our estimate of the Coulomb effects in Eq. (30) and that of Fumstahl [6] (already brought up in Sec. III).

B. Density Dependence of Symmetry Energy

To gain a perspective on the recent microscopic results in the literature [4,6] on skin systematics, we further confront our results from the Thomas-Fermi model to those obtained in the variety of mean-field models explored there. In Fig. 12 the skins from the mean-field calculations [6] are presented vs the reduction factor s for the symmetry energy per nucleon at $\rho=2$ (left panel), vs the scaled derivative of the energy at normal density $p_0 = \frac{2}{\rho} ds/d\rho$ (center panel) and vs the volume symmetry parameter β (right panel). The skin dependence on p_0 and on β was explored in [6]. A similar derivative to p_0 was utilized in [4,5]. It is apparent in each panel of Fig. 12, that the Thomas-Fermi model, represented by lines, produces the general trends such as found in the mean-field calculations, represented by symbols. However, in the three panels, the represented dependencies for the skins in the Thomas-Fermi model are of a quite different nature. Thus β has a very limited bearing on the skins in (30), just through a rescaling of the Coulomb corrections. However, when β is correlated with $=$ through the binding-energy requirements, the changes in β force

changes in α and, thus, produce significant changes in the skin in the rightmost panel of Fig. 12. In the center panel for the Thomas-Fermi model, we observe combined indirect and direct (albeit at the edge of the relevant density interval) effects of the abscissa on the skin. Only in the leftmost panel for the Thomas-Fermi model, we observe the effect of a direct physical connection between the abscissa and the skin through Eqs. (30) and (62). The three panels illustrate dangers of scouting for a physical relation [46] while following numerical results within models that are necessarily constricted.

For a given effective interaction, the mean-field models yield certainly more realistic results in the surface region than the Thomas-Fermi model. However, there is no reason to believe that a strong primary sensitivity of the symmetry parameter ratio α to the density dependence of s disappears in the mean-field models. Using the results for the ^{208}Pb skins [6] in those models, we can assess α for the models from (30) and produce constraints on the low-density s from the constraints on α . An alternative would be to use the data on ^{208}Pb skins directly to constrain s in Fig. 12. The values of s at $\rho=2$ vs α from inverting (30) for the mean-field models are shown in Fig. 13. Basing here the results on one heavy nucleus, we augment, in the inversion, the Coulomb correction in (30) by 0.03 fm; notably an ad hoc procedure for all nuclei might be to amplify the Coulomb correction by a factor of 1.4. Given the variation of the results in Fig. 13, for the acceptable range of 2:1, $\alpha = 0.32$, we deduce the range of the symmetry energy reduction factor at $\rho=2$ of 0.56 to 0.81.

C. Skin Size vs Difference of Separation Energies?

A strong dependence of the sizes of asymmetry skins on the difference of separation energies between protons and neutrons was predicted within the mean-field calculations of Ref. [35]. The dependence has been observed experimentally [21] and it was referred to in other mean-field calculations [36,4]. As we shall demonstrate, for describing the average features of the dependence, a macroscopic model suffices. Interestingly, the dependence allows for a direct access to the surface symmetry parameter α .

The separation energy difference, up to a factor and $O(A^{-1})$ effects, is nothing else but the asymmetry chemical potential α_a . From the energy contributions (12) and (17), we get right away

$$\alpha_a = \frac{\partial E}{\partial (N_S - Z_S)} = \frac{2(N_S - Z_S)}{A^{2/3}} - \frac{5}{6} a_C \frac{Z}{A^{1/3}} : \quad (63)$$

The difference of sharp-sphere radii (26) can be then written in terms of the chemical potential as

$$\frac{R_n - R_p}{R} = \frac{A}{6N} (N_S - Z_S) = \frac{\alpha_a}{12} \frac{A^{5/3}}{N Z} + \frac{5}{72} \frac{a_C}{N} \frac{A^{4/3}}{Z} : \quad (64)$$

With (29), the usefulness correction and with $\alpha_a = (S_p - S_n)/2$ where S_p and S_n are the proton and neutron separation energies, we find

$$\frac{hr^2 i_n^{1/2} - hr^2 i_p^{1/2}}{hr^2 i^{1/2}} = \frac{S_p - S_n}{24} \frac{A^{5/3}}{N Z} - \frac{a_C}{168} \frac{A^{5/3}}{N} - 1 - \frac{35}{3} \frac{1}{A^{1/3}} + \frac{2}{hr^2 i} \frac{d(d_n - d_p)}{hr^2 i} : \quad (65)$$

In the analysis of data, so far, the surface symmetry parameter always came in a combination with the parameter α . However, the situation is different with the dependence of the skin size on the separation energy difference. According to the relation (65), in a given mass region, the skin size is largely linear in the separation energy, with the slope inversely proportional to α . The parameter α appears only within the Coulomb correction in the relation. As we have by now analyzed both the binding energies and skins vs the mass and charge numbers in terms of the symmetry parameters, the analysis of data on the skins vs energies need not inject a new information. However, we can use the relation in checking locally the results of global fits. From the results of global fits on $\alpha = 1$, we deduce $10.0 \text{ MeV} \dots 12.5 \text{ MeV}$. In Fig. 14, we show the dependence of skin size on separation-energy difference for sodium isotopes. The best description of the data [21] is obtained for $\alpha = 10.3 \text{ (} 1.0\text{)} \text{ MeV}$, in consistency with the results from global fits.

V I. CONCLUSIONS

Macroscopic nuclear properties have been discussed in terms of the symmetry energy volume and surface parameters. The need for a surface symmetry parameter is apparent in the binding energy systematics for light nuclei with a significant nucleon asymmetry. In a consistent treatment of the nuclear energy, the nuclear surface is viewed as providing an additional capacitance for the nucleon asymmetry of $2A^{2/3} = \dots$ in addition to the volume capacitance of $2A = \dots$. The energies associated with the surface and the interior combine in the energy formula like energies of two capacitors in parallel. The requirement that the parameter combination in the energy formula reproduces the standard symmetry coefficient for heavy nuclei, with the large asymmetries, imposes a strong correlation between the value of the volume parameter and the parameter ratio $\alpha = \dots$.

An excess capacitance of the nuclear surface for asymmetry leads to a difference of sharp-sphere and of rms radii for neutrons and protons, or skin effect. For a given relative asymmetry, in the macroscopic considerations, the skin size in terms of radii has a nontrivial behavior on the nuclear mass; it first increases as the mass increases, then turns to a constant, to get finally eroded by Coulomb effects.

The existing data on asymmetry skins, together with the binding-energy data, permit to establish limits of $27 \text{ MeV} \dots 32 \text{ MeV}$ for the volume symmetry parameter, $10.0 \text{ MeV} \dots 12.5 \text{ MeV}$ for the surface parameter and $\alpha = 1.1 \dots 3.2$ for the ratio. Given the ratio assessment, the ratio of the net asymmetry in the surface to the asymmetry in the volume, equal to $\alpha = A^{1/3}$, can be of order of 1 for light nuclei. For reference, when taking the parameter ratio in the middle of the permitted range, $\alpha = 2.6$, the sample best-fit parameter values in describing the binding energies with (20) and (21) are $a_V = 15.47 \text{ MeV}$, $a_S = 18.42 \text{ MeV}$, $a_C = 0.694 \text{ MeV}$, $a_P = 9.84 \text{ MeV}$, $\alpha = 29.70 \text{ MeV}$ and $\beta = 11.42 \text{ MeV}$. When ignoring the surface usefulness in putting $\alpha = 0$ in (20), the best-fit values are $a_V = 15.60 \text{ MeV}$, $a_S = 18.01 \text{ MeV}$, $a_C = 0.691 \text{ MeV}$, $a_P = 10.11 \text{ MeV}$, $\alpha = 33.40 \text{ MeV}$ and $\beta = 12.85 \text{ MeV}$.

With inclusion of the surface capacitance in description of the collective modes of asymmetry vibration, the modes evolve in their character, as nuclear mass increases, from more Goldhaber-Teller like to more Steinwedel-Jensen like. The changes get reflected in the dependence of mode energy on mass and in the transition density.

Within the Thomas-Fermi considerations, the additional surface capacitance is associated with a drop of the symmetry energy per nucleon S with density. (Indeed, $2=S$ represents the capacitance per nucleon.) The utilized Thomas-Fermi model allows to test the phenomenological assessment of asymmetry skins. For light nuclei the agreement between the assessed and calculated directly is remarkable, but for heavy nuclei a small but systematic discrepancy develops attributed to Coulomb interactions. Using the results on mean-field models in the literature and the range for the symmetry-parameter ratio, the drop in the symmetry energy at half the normal density, compared to normal, is estimated to be within the range 0.56 . s . 0.81.

ACKNOWLEDGMENTS

The hospitality extended by the Nuclear Theory Group of the Tohoku University, where this work was initiated, is gratefully acknowledged. Acknowledged is further a collaboration, on a topic related to the present work, with Sergio Souza and Betty Tang. Betty, in particular, suggested an early version of Fig. 4. A discussion with Bill Lynch helped in clarifying an issue in Sec. II. Naffali Auerbach provided explanations on giant resonances and Stefan Typel and Michael Thoennessen helped in identifying some relevant literature. Finally, Dick Fumstahl generously supplied unpublished details of his calculations [6], employed in Figs. 12 and 13. This work was partially supported by the National Science Foundation under Grants PHY-0070818 and INT-0124186.

REFERENCES

[1] Isospin Physics in Heavy-Ion Collisions at Intermediate Energies, eds. B .A .Li and U . Schroder, ISBN 1-56072-888-4 (Nova Science Publishers Inc., New York, 2001).

[2] J. M .Lattimer and M .Prakash, *Astrophys. J.* 550, 426 (2001).

[3] K .Oyamatsu, I .Tanihata, Y .Sugahara, K .Sumiyoshi and H .Toki, *Nucl. Phys. A* 634, 3 (1998).

[4] B .A .Brown, *Phys. Rev. Lett.* 85, 5296 (2000).

[5] S .Typel and B .A .Brown, *Phys. Rev. C* 64, 027302 (2001).

[6] R .J .Furnstahl, *Nucl. Phys. A* 706, 85 (2002).

[7] C .F .Weizsäcker, *Zeit. f. Phys.* 96, 431 (1935).

[8] H .A .Bethe and R .F .Bacher, *Rev. Mod. Phys.* 8, 82 (1936).

[9] J. W . Gibbs, *The Collected Works*, Yale Univ. Press, New Haven, 1948.

[10] W .D .Mayers and W .J .Swiatecki, *Ann. of Phys.* 55, 395 (1969).

[11] W .D .Mayers, W .J .Swiatecki and C .S .Wang, *Nucl. Phys. A* 436, 185 (1985).

[12] W .D .Mayers and W .J .Swiatecki, *Phys. Rev. C* 63, 034318 (2001).

[13] M .Goldhaber and E .Teller, *Phys. Rev.* 74, 1046 (1948).

[14] H .Steinwedel and H .Jensen, *Z. Naturforschung 5A*, 413 (1950).

[15] G . Audi and A . H .Wapstra, *Nucl. Phys. A* 595, 409 (1995),
<http://www.nndc.bnl.gov/nndc/nndc/masses>

[16] L .Ray, *Phys. Rev. C* 19, 1855 (1979).

[17] S .Shlomo and R .Schaefer, *Phys. Lett. B* 83, 5 (1979).

[18] C .J .Batty, E .Friedman, H .J .Gils and H .Rebel, *Advances in Nuclear Physics*, vol. 19, ed. J. W .Negele, (Plenum Press, New York, 1989) p. 1, and refs. therein.

[19] W .R .Gibbs and J .P .Dedonder, *Phys. Rev. C* 46, 1825 (1992).

[20] V .E .Starodubsky and N .M .Hintz, *Phys. Rev. C* 49, 2118 (1994).

[21] T .Suzuki et al., *Phys. Rev. Lett.* 75, 3241 (1995).

[22] S .Karatzagidis, K .Amos, B .A .Brown and P .K .Dob, *Phys. Rev. C* 65, 044306 (2002).

[23] B .C .Clark, L .J .Kerr and S .Ham a, *nucl-th/0209052*.

[24] C .W .de Jager, H .de Vries, and C .de Vries, *Atomic Data and Nuclear Data Tables* 14, 479 (1974).

[25] C .J .Horowitz and J .P .iekarewicz, *Phys. Rev. Lett.* 86, 5647 (2001); *Phys. Rev. C* 64, 064616 (2001); *Phys. Rev. C* 66, 055803 (2002).

[26] C .J .Horowitz, S .J .Pollock, P .A .Souder and R .M .Michaels, *Phys. Rev. C* 63, 025501 (2001).

[27] S .S .Dietrich and B .L .Berman, *Atomic Data and Nuclear Data Tables* 38, 199 (1988).

[28] R .P .Ittman et al., *Phys. Rev. C* 19, 1251 (1979).

[29] P .Ring and P .Schuck, *The Nuclear Many-Body Problem* (Springer-Verlag, New York, 1980).

[30] A .Bohr and B .R .Mottelson, *Nuclear Structure* (Benjamin, New York, 1975), Vol. II.

[31] W .D .Mayers, W .J .Swiatecki, T .Kodama, L .J .ElJaick and E .R .Hilf, *Phys. Rev. C* 15, 2032 (1977).

[32] D .Pines and Ph .Nozieres, *The Theory of Quantum Liquids* (Benjamin, New York, 1966).

[33] S .Khamerdzhiev, J .Speth and G .Tertychny, *Nucl. Phys. A* 624, 328 (1997).

[34] P .Danielewicz, *Nucl. Phys. A* 673, 375 (2000).

[35] I. Tanihata et al, *Phys. Lett. B* 289, 261 (1992).

[36] B .A .B rown and W .A .R ichter, *Phys. Rev. C* 54, 673 (1996).

FIGURES

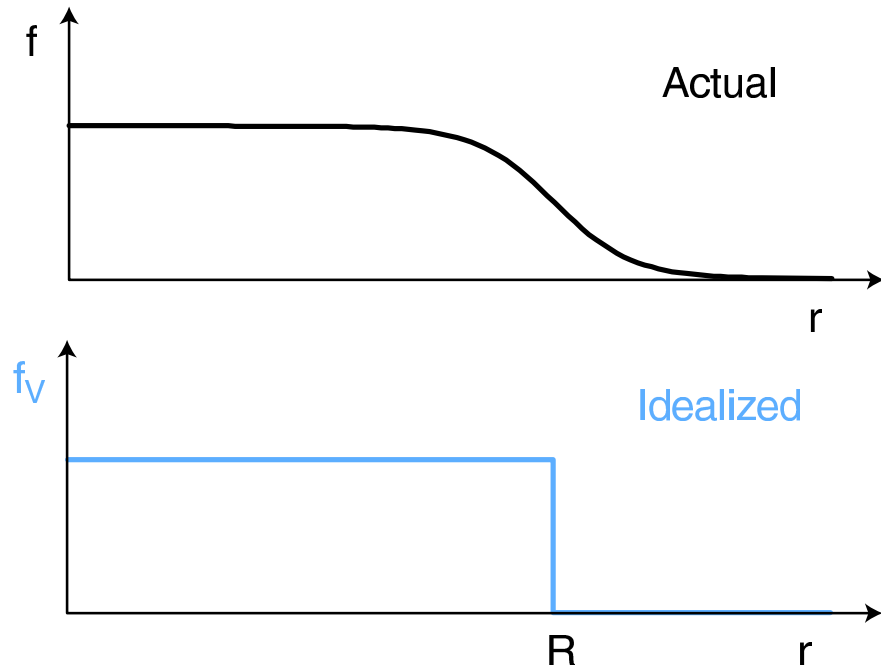


FIG. 1. Illustration for the construction of surface quantities following Gibbs [9]. The top shows the variation of the density f for some quantity F within the system. The bottom shows an idealized reference system, where the density changes in a discontinuous manner, right at the surface, between the density values f_V characteristic for the system away from the interface. The surface quantities F_S are defined as the difference between F for a macroscopic volume containing the interface and F_{id} for the same volume in the reference system, $F_S = F - F_{id}$.

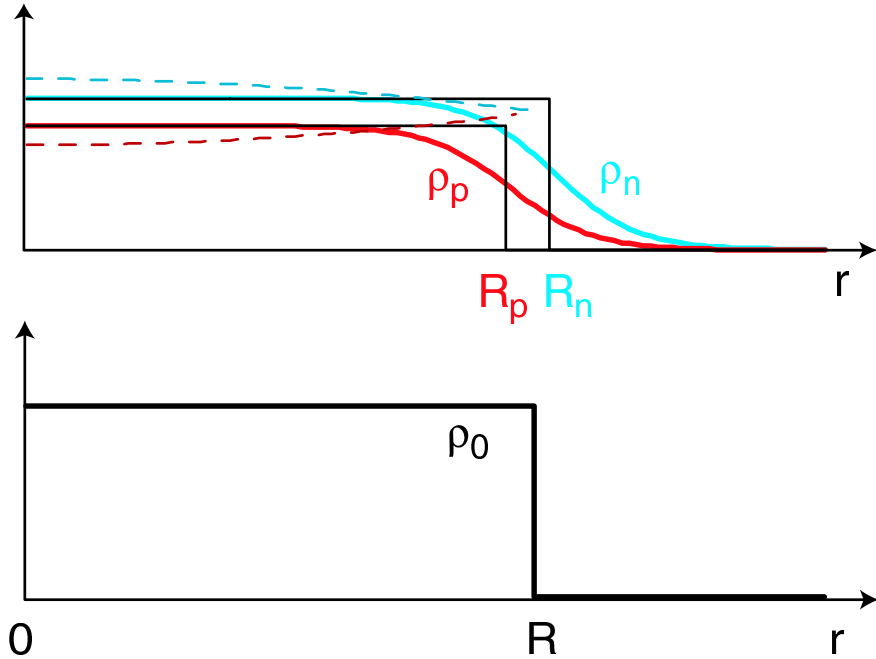


FIG. 2. In a two-component system, the surface-attributable particle-asymmetry can arise even when the surface is constructed to have no net particle number. For a spherical ground-state nucleus, this corresponds to the situation when the sharp-sphere equivalent proton radius R_p and neutron radius R_n differ from each other and bracket the matter sharp-sphere radius R . The dashed lines in the top part of the figure illustrate the polarization of a nuclear interior, in the form of a sharp-edged sphere of radius R , by the Coulomb interactions.

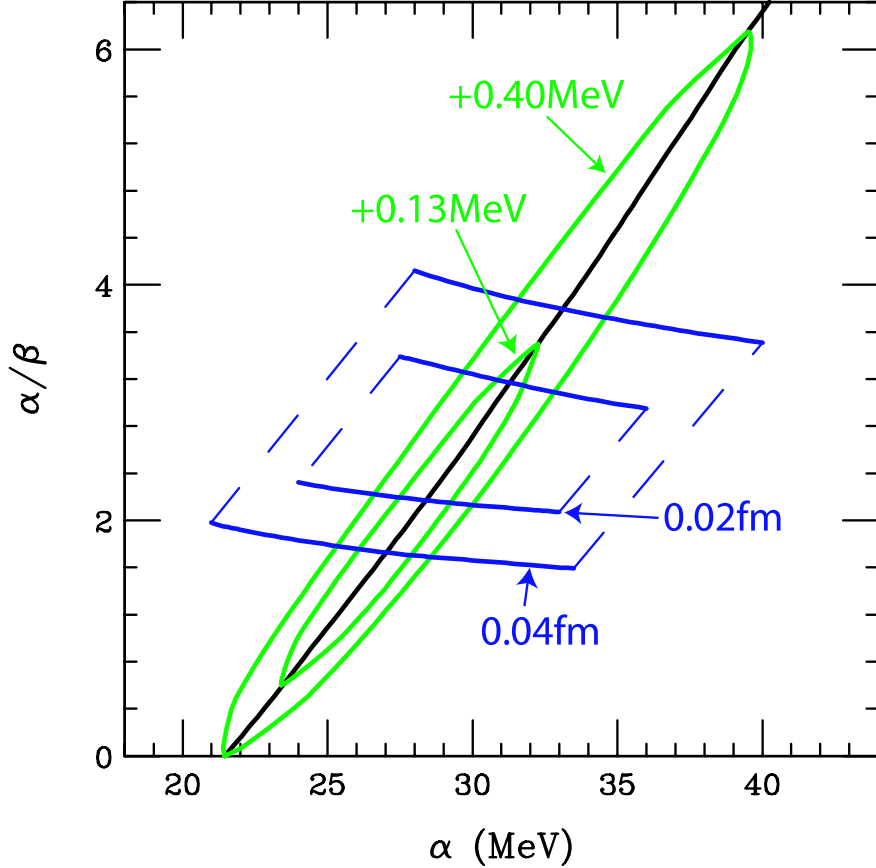


FIG . 3. Results from optimizations of the volume parameter and the volume-to-surface parameter ratio α/β . The thick solid diagonal line shows the optimal values of α and α/β when fitting the nuclear masses. The oval contour lines show the loci of parameter combinations that yield average absolute deviations from the measured nuclear masses larger by 0.13 and 0.40 MeV, respectively, than the best-fit parameter combination. The rectangular contour lines indicate the loci of parameter combinations at constant χ^2 when fitting the asymmetry skins deduced from data. The loci are for the χ^2 -values assuming the combination of a standard statistical deviation and an average systematic error of the skin-size formula of 0.02 and 0.04 fm, respectively. Only the solid more horizontal portions of the skin-thickness contours are meaningful { the portions paralleling the binding energy correlation serve to guide the eye only.

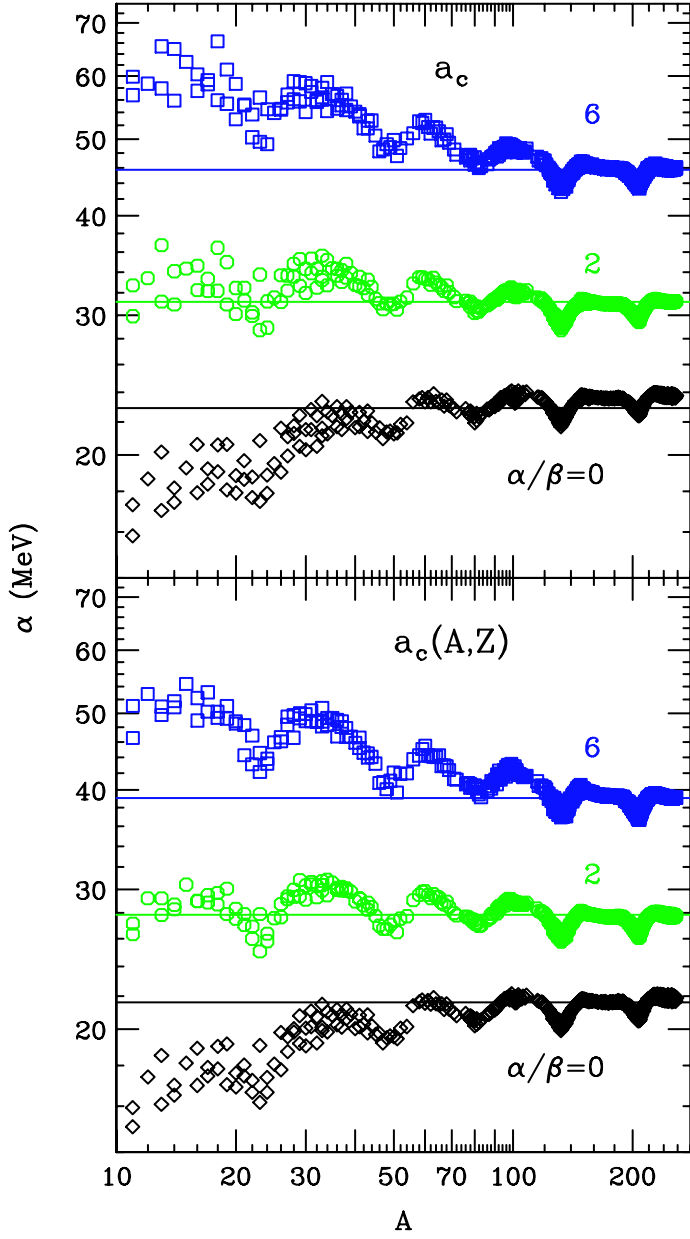


FIG. 4. Values of the volume symmetry parameter α (MeV) from inverting the energy formula at different values of α_c , for individual nuclei with $|N - Z|/A > 0.2$, as a function of A . The top panel shows results for the energy formula with $\alpha_c = 0$ and the bottom for the formula with α_c given by Eq. (21). The different symbols represent results from the inversion for $\alpha_c = 6$ (squares), 2 (circles) and 0 (diamonds), respectively. The horizontal lines represent values of α from the global fits at the different α_c .

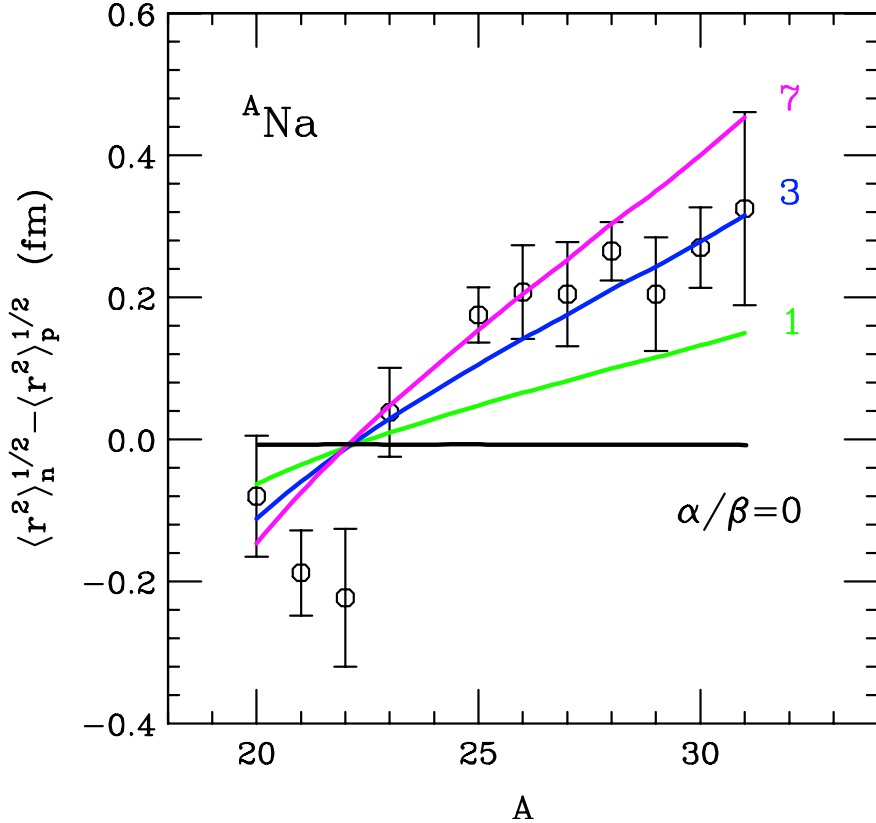


FIG. 5. Difference between the neutron and proton rms radii for Na isotopes as a function of the mass number. The symbols represent results from the data analysis Ref. [21]. The different lines represent results from Eq. (30) for the indicated values of γ , $d_n - d_p = 0$ and α/β taken from the binding-energy correlation valley in Fig. 3.

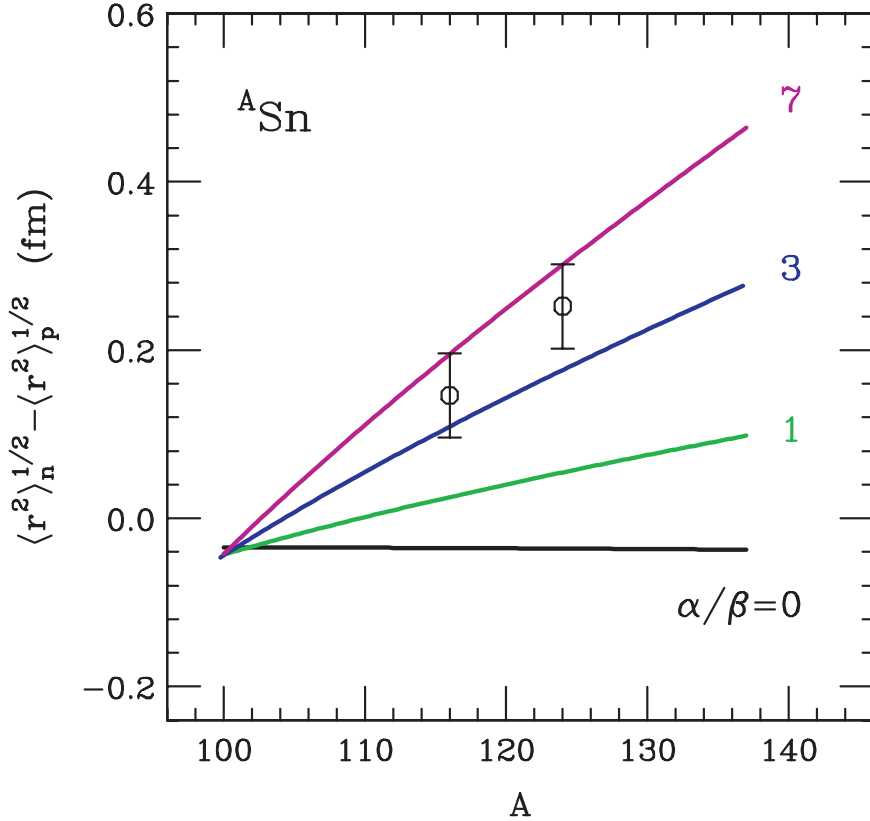


FIG. 6. Difference between the neutron and proton rms radii for Sn isotopes as a function of the mass number. The symbols represent results from the data analysis of Ref. [16]. The different lines represent results from Eq. (30) for the indicated values of α/β , $d_n - d_p = 0$ and α/β taken from the binding-energy correlation valley in Fig. 3.

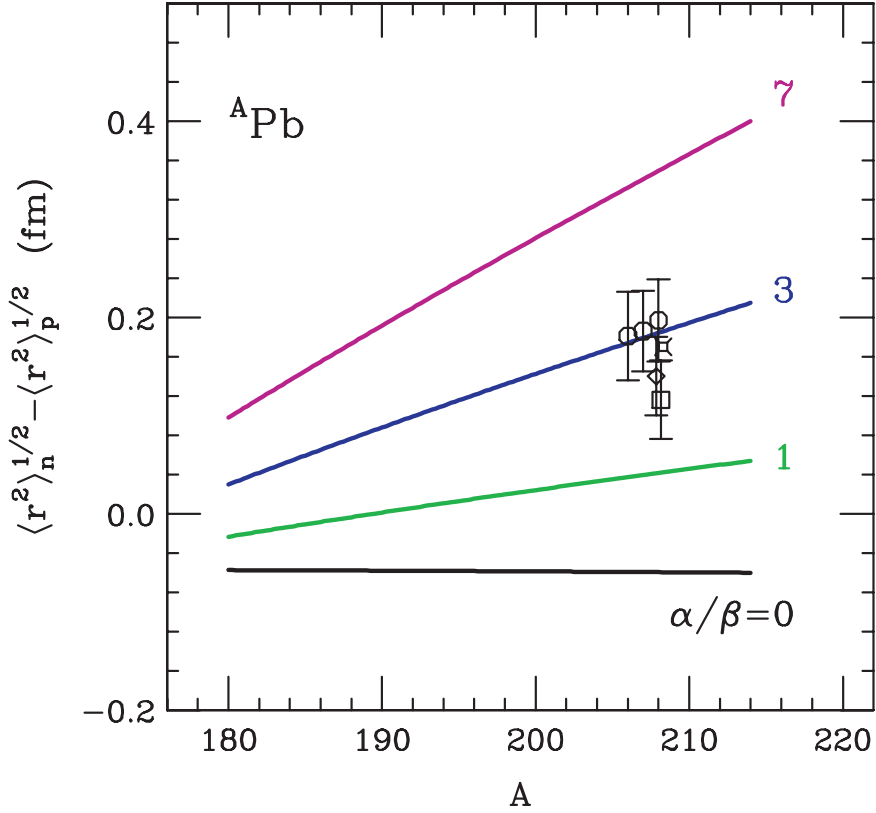


FIG. 7. Difference between the neutron and proton rms radii for Pb isotopes as a function of the mass number. The symbols represent results from the data analysis of Refs. [20] (circles), [16] (a diamond), [23] (a square) and [22] (a cross). The different lines represent results from Eq. (30) for the indicated values of α , d_n , d_p = 0 and β taken from the binding-energy correlation valley in Fig. 3.

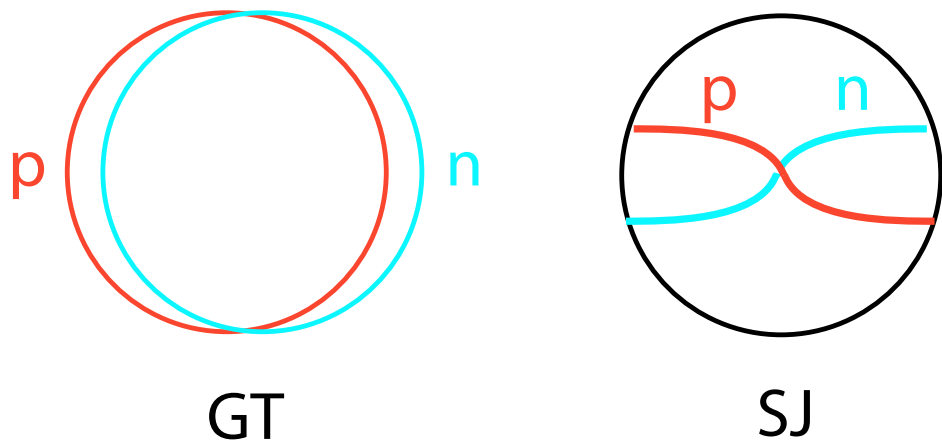


FIG. 8. In the GT model [13] of the GDR, the neutron and proton distributions are assumed to oscillate, unchanged with respect to their centers, against each other. In the SJ model [13,14] of the GDR, the particle asymmetry oscillates with in the nuclear interior, with flux of the asymmetry vanishing at the nuclear surface.

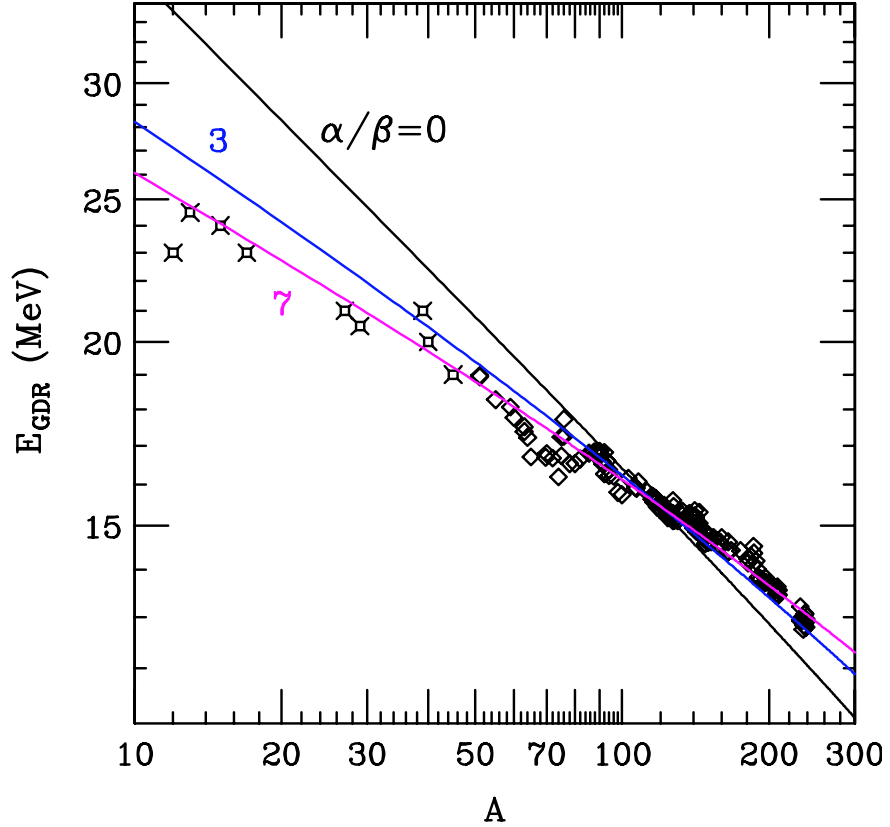


FIG. 9. Energy of the giant dipole resonance as a function of the mass number A . Symbols represent photoabsorption data from the compilation [27]. For mass numbers $A > 50$, we use the energies from the Lorentzian function fits from [27]. When a splitting characteristic for a deformed nucleus is present, we plot the equivalent energy for a spherical nucleus. For mass numbers $A < 50$, we plot the peak values for nuclei for which a clear isolated peak is present in the photoabsorption cross section [27]. The lines represent energies calculated from $E_{GDR} = (2^p (N-Z)/A) \sim c_a q_{11}$ with c_a being a fit parameter and with q_{11} obtained from (47) at different indicated values of α/β .

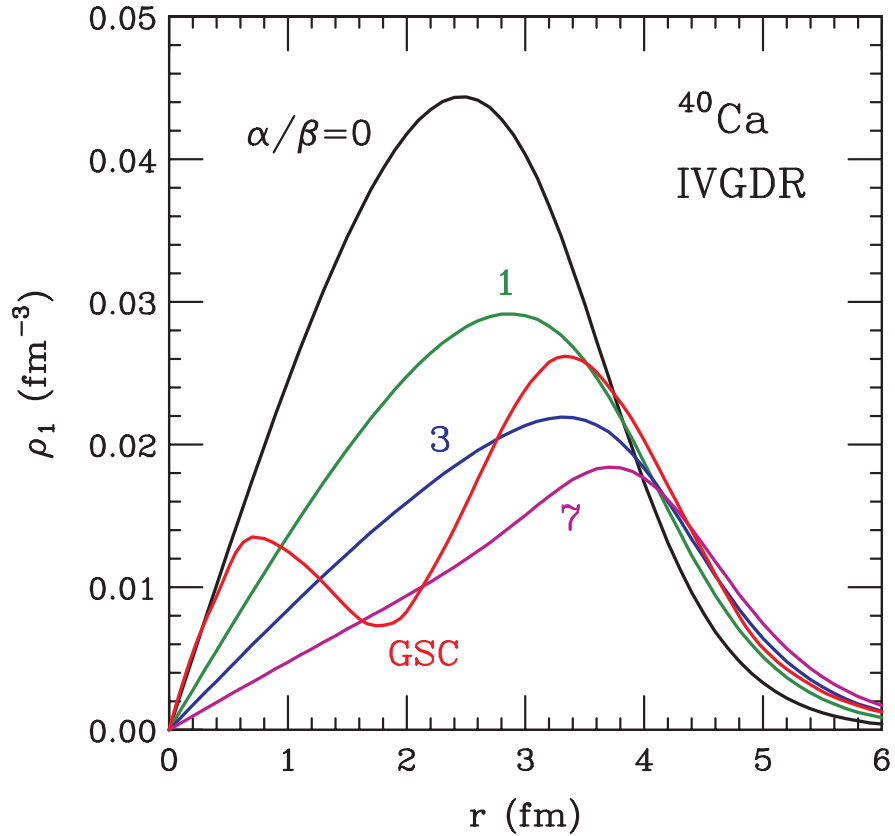


FIG. 10. GDR transition density ρ_1 for ^{40}Ca , as a function of the distance r from the nuclear center. The lines marked with the respective values of the parameter ratio α/β represent the densities obtained from Eq. (52). The line marked GSC represents the density from the microscopic calculations of Ref. [33] including the effects of 2p-2h excitations and of ground-state correlations.

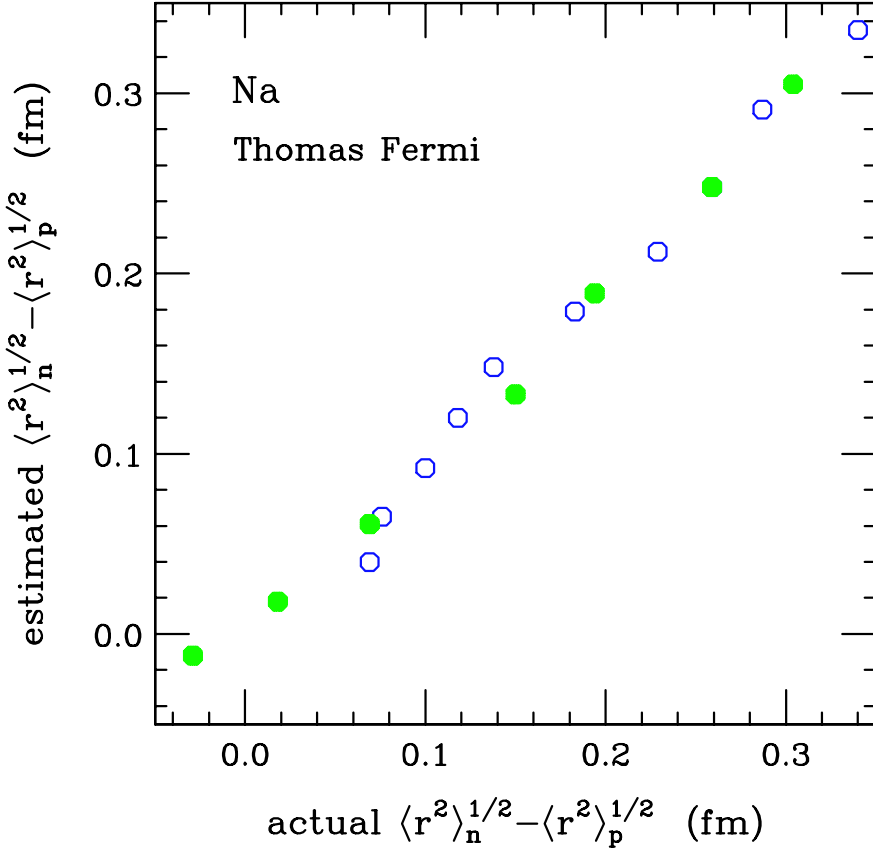


FIG. 11. Size of the asymmetry skin estimated with Eq. (30) vs size obtained directly from the calculated nucleon distributions, within the Thomas-Fermi calculations of sodium isotopes. The filled circles represent the results for $\alpha = 3$, while changing the isotope mass. The open circles represent the results for ^{30}Na , while changing the values of α and correlating the changes in to follow the valley in Fig. 3.

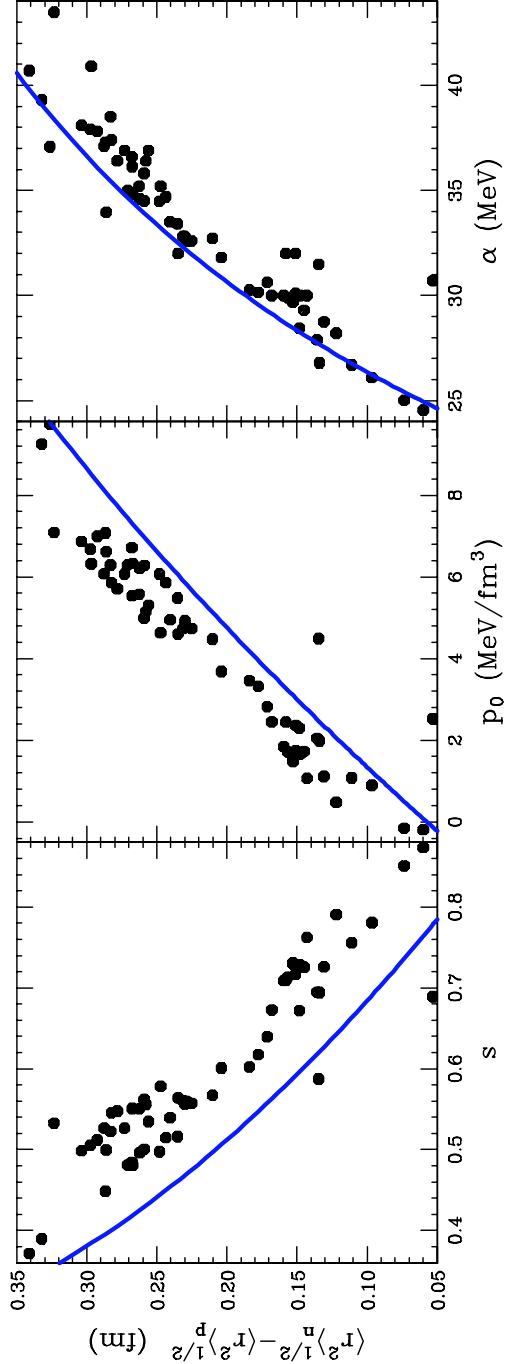


FIG. 12. Size of the asymmetry skin in models vs the reduction factor s for the symmetry energy at $s_0=2$ (left panel), vs the scaled derivative [3,6] of the energy $p_0 = \frac{2}{s_0} (dS/ds)$ at s_0 (center panel) and vs the volume symmetry parameter α (right panel). Symbols indicate results for a variety of mean-field models explored by Fumstahl [6]. Lines indicate Thomas-Fermi results, from Eq. (30) using (62).

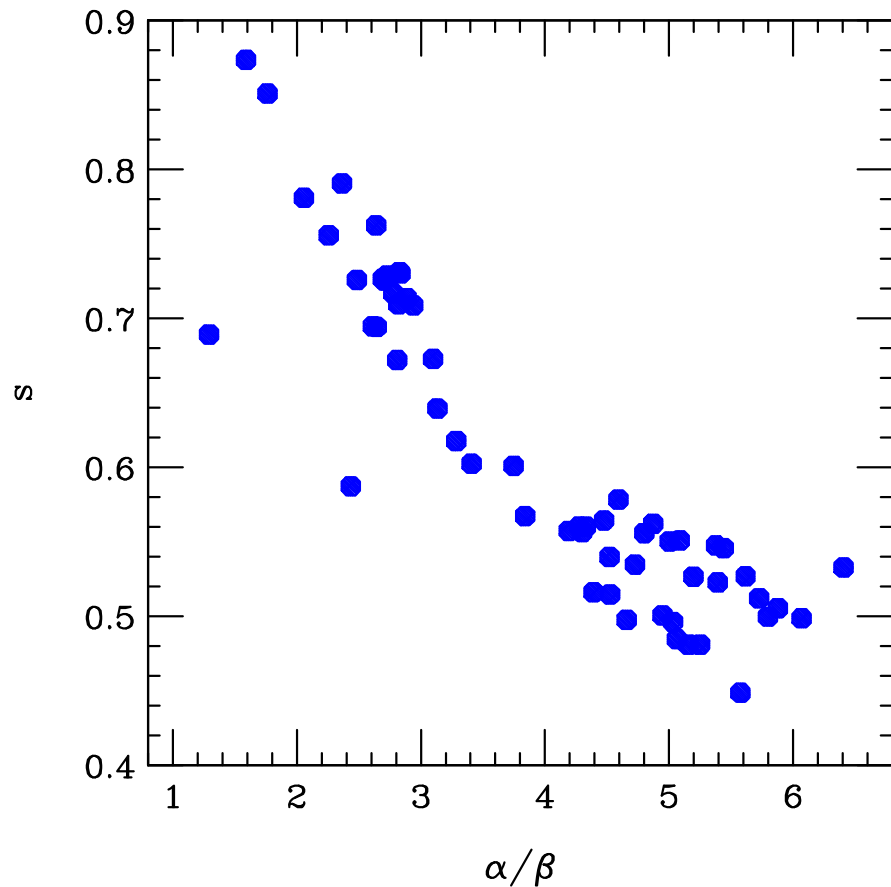


FIG. 13. Reduction factor s for the symmetry energy per nucleon at $\theta=2$ vs the symmetry parameter ratio α/β deduced for the mean-field models from the calculated [6] ^{208}Pb skins and Eq. (30).

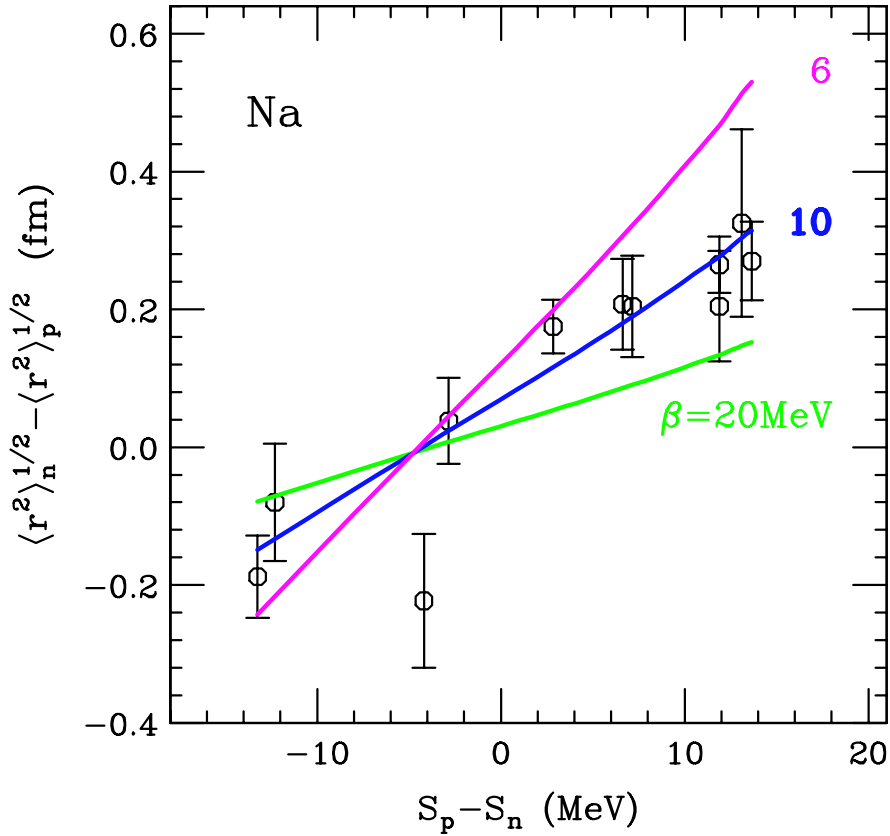


FIG. 14. Difference between the neutron and proton mean radii vs the difference between the proton and neutron separation energies for Na isotopes. The symbols represent data of Ref. [21]. The lines represent predictions of Eq. (65) for different indicated values of β (in MeV) with the values of β made to follow the binding-energy correlation in Fig. 3.